JOURNAL OF THERMOPHYSICS AND HEAT TRANSFER
Vol. 25, No. 3, July–September 2011

Thermal Cracking and Heat Sink Capacity of Aviation Kerosene Under Supercritical Conditions

Fengquan Zhong,* Xuejun Fan,† Gong Yu,† and Jianguo Li†
Chinese Academy of Sciences, Beijing 100190, People's Republic of China
and
Chih-Jen Sung‡
University of Connecticut, Storrs, Connecticut 06269

DOI: 10.2514/1.51399

Thermal cracking and endothermicity of China No. 3 aviation kerosene were studied experimentally under supercritical conditions relevant to regenerative cooling systems for scramjet applications. A multiple-stage heating system with reaction products collection was used that can achieve a fuel temperature range of 780–1050 K, a pressure range of 3–4.5 MPa, and a residence time range of 0.6–3 s. The chemical heat sink was determined through a control volume analysis of the fuel flow. Compositions of the cracked gaseous and liquid products were analyzed via gas chromatography. Based on the results of fuel conversion, the temperature range for the active cracking was observed to be approximately 800–1000 K, beyond which the cracking approaches completion. It was also found that the variation of the chemical heat sink with temperature can be nonmonotonic and a maximum endothermicity was seen to occur in the temperature range of 900–960 K, depending on the residence time. For the current operation conditions, the maximum chemical heat sink reached 0.5 MJ/kg at a fuel conversion of 45%. Composition analysis of the gaseous product indicated that the saturated hydrocarbons such as methane became dominant as temperature was increased. On the other hand, the major compositions of the liquid product were benzene-based and naphthalene-based hydrocarbons.

I. Introduction

FOR hypersonic applications, active cooling using onboard hydrocarbon fuel is considered to be one of the most effective ways for thermal protection. Before injection into combustor, the fuel flows through cooling channels along the engine liner, carrying away heat from the wall via heat convection and endothermic reactions. For high Mach number flight, the sensible heat of the fuel is no longer adequate for the cooling requirement and an extra heat sink is required, which can be provided by endothermic cracking of the fuel at high temperatures [1,2].

Thermal cracking of hydrocarbon and its applications have been studied broadly in petrochemical industry [3], of which the working pressure is near atmospheric pressure and much lower than the pressures for hypersonic application. For example, the typical pressure in the cooling channel of a Mach-6 scramjet is approximately 4–7 MPa, higher than the critical pressure (∼2 MPa) for most liquid hydrocarbons. Compared with low pressure cracking, high-pressure situations are expected to lead to lower fuel conversion, larger percentage of paraffin products, and less endothermicity, while keeping other operating conditions the same. Hence, it is imperative to study characteristics of thermal cracking of hydrocarbons and the associated endothermicity under supercritical pressures.

Lander and Nixon [1] discussed properties and possible cooling applications of thermal and catalytic cracking of various hydrocarbons. They found that the chemical heat sink due to thermal cracking did not always increase with temperature. For JP-7 fuel, the maximum endothermicity was approximately 0.72 MJ/kg at a 60% conversion. Edwards and Anderson [4] studied thermal cracking of JP-7 fuel through a heated tube system and found that the endothermicity of JP-7 was on the order of 0.7 MJ/kg, which is much smaller than the theoretical value (3.5 MJ/kg) if assuming the cracking products were all alkenes such as ethylene. Based on the results of gas and mass chromatograph, they [4] argued that the reduction in the endothermicity was caused by significant formation of saturated hydrocarbons. Edwards [5] further showed that the flow reactor residence time is critical for the endothermic property of the cracking mixture, since long residence time would form products approaching the equilibrium products such as light saturated hydrocarbons and the overall reactions become exothermic. As discussed in [5,6], the effect of residence time could be easily characterized by plotting olefin/paraffin ratio (an indicator of endothermicity) as a function of residence time. In general, shorter residence time corresponds to larger olefin/paraffin ratio, thereby leading to a more endothermic cracking process. Stewart et al. [7] studied pyrolysis of *n*-decane and decalin at temperatures of 700–810 K and subcritical/supercritical pressures of 0.2–10 MPa. It was found that the main products of supercritical pyrolysis were different from those from subcritical pyrolysis, and high pressure can promote the C_6 to C_5 ring contraction. Fan et al. [8] investigated supersonic combustion properties of thermally cracked China No. 3 aviation kerosene in a supersonic model combustor. Higher combustion efficiency was found for the cracked kerosene since the cracking products consisting of small molecules such as ethylene and hydrogen that can assist fuel/air mixing and combustion. It is worth mentioning that for most of previous studies, the fuel temperature varied along the reaction section of the heated tube and at the same time, there existed a significant temperature difference between the fuel and the wall, i.e., a somewhat large temperature gradient. Because of the axial and radial temperature gradients within the tube, an accurate cracking temperature is hard to define and the cracking process is coupled with convective heat transfer causing difficulties in interpreting the experimental results. Therefore, one of the objectives of this paper is to obtain a relatively uniform fuel temperature distribution along the reaction section as well as a negligible heat convection effect (i.e.,

Presented as Paper 2009-5267 at the 45th AIAA/ASME/SAE/ASEE Joint Propulsion Conference and Exhibit, Denver, CO, 2–5 August 2009; received 30 June 2010; revision received 1 October 2010; accepted for publication 2 October 2010.

*Associate Professor, Key Laboratory of High Temperature Gas Dynamics, Institute of Mechanics; fzhong@imech.ac.cn (Corresponding Author).

†Professor, Key Laboratory of High Temperature Gas Dynamics, Institute of Mechanics.

‡Professor, Department of Mechanical Engineering. Associate Fellow AIAA.

negligible fuel/wall temperature difference) with a unique multiple-stage heating system.

In this study, thermal cracking of China No. 3 aviation kerosene (a fuel similar to JP-8) was investigated in heated stainless steel tube at varying fuel temperatures (780–1050 K), pressures (3–4.5 MPa), and residence times (0.6–3 s). With directly measured fuel and wall temperatures along the tube and a 10-species fuel surrogate, a heat transfer analysis was applied to determine the chemical heat sink and the associated flow properties. The cracked gas and liquid products were cooled rapidly through a water-cooling system and then collected for the speciation measurements using gas chromatography. Compositions of the gaseous and liquid products were identified for the understanding of the cracking and endothermicity properties. In addition, the fuel conversion and the mass flow rate of the cracked mixture were measured. Furthermore, the current study was aimed at investigating the effects of temperature, pressure, and residence time on the thermal cracking process of aviation kerosene as well as at determining the endothermicity property under conditions relevant to the cooling system for scramjet applications. This work is expected to provide further insight into the cracking property at supercritical pressures and to provide fundamental data for the design and optimization of an effective cooling system of a scramjet.

In the next section, the test facility is described. A heat transfer analysis based on the energy conservation of a control volume is then introduced. In the following section, the cracking results including fuel conversion, chemical heat sink, mass flow rate, and species analysis are presented and discussed. Finally, we summarize the main conclusions that can be drawn from the experimental results.

II. Experimental Facility

A. Kerosene Multiple-Stage Heating System

Figure 1 shows a sketch of the two-stage heating system. The first stage was a storage-type heater, which had a volume of approximately three liters and can preheat the fuel to a maximum temperature of 550 K within 1 h and with negligible carbon deposition. When the preheated fuel was ready, a pneumatic valve controlled by a solenoid valve via computer was opened to turn on the flow. The preheated fuel then flowed through the second stage heater and was heated rapidly. The second heater consisted of 21-meter-long stainless steel tube with an inner diameter of 12 mm and a wall thickness of 2 mm. The tube was heated by heating tapes with a maximum power of 12 kW and each tape can be controlled independently to achieve a uniform wall temperature of the heater. With asbestos insulation, the second stage heater can easily heat the kerosene to a temperature of higher than 1000 K. Part of the second stage heater served as the test section for the cracking reactions at a relatively uniform temperature distribution.

Pressures at the inlet and outlet of the second stage heater were measured with pressure transducers. A uniqueness of the current facility is that in the second stage heater, both the wall and fuel temperatures were simultaneously measured at the same location along the flowpath. There were 16 Type-K thermocouples spot-welded on the outer wall surface of the tube for the measurement of the outer wall temperature and 16 Type-K sheath thermocouples mounted through the tube wall and positioned at approximately the tube centerline for the measurement of the bulk fuel temperature. The fuel thermocouple was installed with a steel tube filled with zirconium dioxide to prevent heat conduction from the wall to the thermocouple sheath. Details of the fuel thermocouple assembly and alignment can be found in [9]. The uncertainty associated with the wall/fuel temperature measurement was estimated to be less than ± 3 K, while that in the pressure measurements was less than 0.5%.

B. Fuel Control and Collection System

Schematic diagram of the fuel control and collection system is shown in Fig. 2. A sonic nozzle flow meter was installed downstream of the test section to determine the fuel mass flow rate by using the calibration method proposed in our previous studies [10,11]. Sonic nozzles with three throat diameters (1.6, 2.55, and 3.08 mm) were used to obtain different mass flow rate ranges, resulting in different residence times for the same heating tube system. In this work, the effect of residence time on thermal cracking is of primary interest. For the current system, the fuel mass flow rate was in a range of 10–100 g/s, corresponding to residence times of approximately 0.3–3 s.

After the sonic nozzle, the heated kerosene along with cracking products was cooled down rapidly to room temperature through a water-cooling system. The gaseous and liquid products were then collected and their compositions were analyzed using gas chromatography. The fuel control and collection system has been used and described in [11,12].

III. Heat Transfer Analysis

The chemical heat sink due to endothermic cracking can be determined by energy analysis of a control volume of the fuel. As

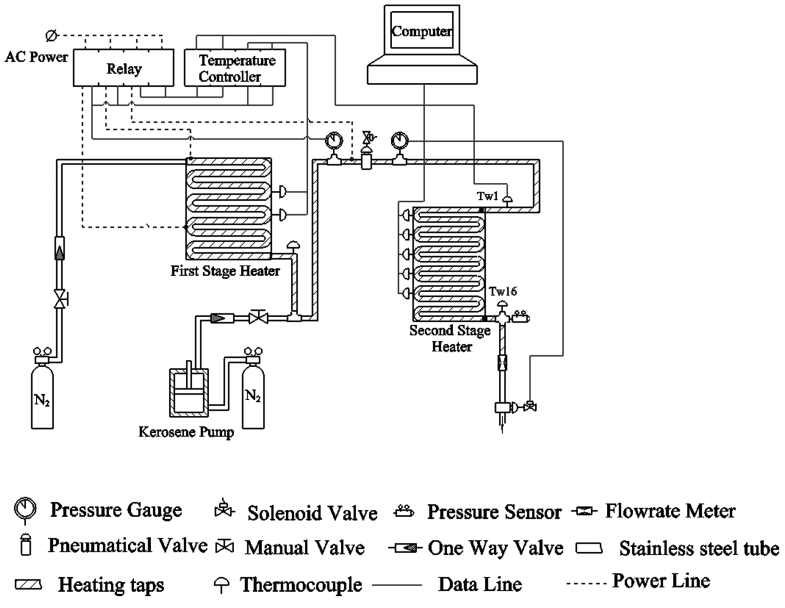

Fig. 1 Schematic diagram of the two-stage heating system.

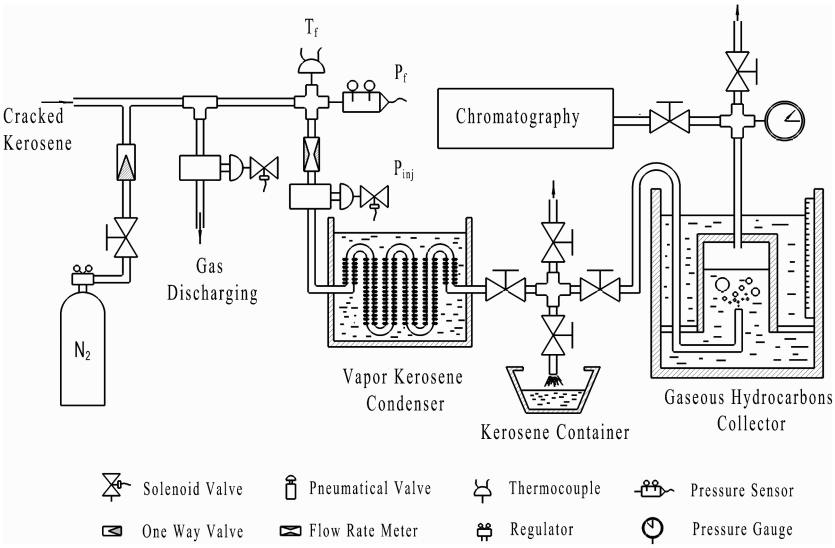

Fig. 2 Sketch of the cracking products collection system.

shown in Fig. 3a, the total heat absorbed by the fuel, Q_{sink} can be calculated when the distribution of wall heat flux $q_w(x)$ is known. And the sensible heat sink ΔH_{sen} of the fuel equals the enthalpy change due to the increase in the fuel temperature. With the notations in Fig. 3a, it yields

$$Q_{\text{sink}} = \pi d_2 \int_0^L q_w(x)\,\mathrm{d}x \tag{1}$$

$$\Delta H_{\text{sen}} = \dot{m}(h(T_L) - h(T_0)) \tag{2}$$

where d_2 is the inner diameter of the tube, $\dot{m}$ is the mass flow rate, and T_0 and T_L are the fuel temperatures at the inlet and outlet of the reaction section, respectively. The fuel enthalpy h can be calculated by National Institute of Standards and Technology *Supertrapp* [13] with a 10-species fuel surrogate as described in [9]. It was found that the sensible heat calculated by Eq. (2) is quite small compared with the total heat sink Q_{sink} because of the small change in the fuel temperature along the test section.

The chemical heat sink can be calculated by,

$$\Delta h_{\text{endo}} = \frac{Q_{\text{sink}} - \Delta H_{\text{sen}}}{\dot{m}} \tag{3}$$

The wall heat flux $q_w(x)$ is calculated as follows. During the experimental run, the power of the second stage heater was off. Thus, $q_w(x)$ can be determined by the rate of the change in the measured wall temperature since the wall temperature decreased as the fuel flowed and carried away heat. As shown in Fig. 3b, considering a control volume of the tube wall enclosed by two adjacent wall temperature measurements and by neglecting the kinetic energy and viscous effect, the energy equation is

$$\frac{\partial \int_V (\rho_w e)\,\mathrm{d}V}{\partial t} + \int_{s_A+s_B} \mathbf{q}_w \cdot \mathbf{n}\,\mathrm{d}s = 0 \tag{4}$$

where ρ_w denotes density of the tube wall and e is the internal energy. The heat flux is defined to be positive when pointing out of the wall surface.

Since the wall outer surface S_B has been well insulated, the heat flux through it can be neglected. Also due to a large ratio of the tube length to its thickness, the heat conduction in the axis direction is negligible. Thus, Eq. (4) reduces to

$$q_w S = -\Delta M C p_w \frac{\partial \bar{T}_w}{\partial t} \tag{5}$$

where $\bar{T}_w = \frac{1}{2}(T_{w1} + T_{w2})$ is the average wall temperature of two adjacent measurements, Cp_w is the specific heat capacity of the wall, $S = \pi d_2 \Delta L$, $\Delta M = \rho_w \frac{\pi}{4}(d_1^2 - d_2^2)\Delta L$ is the mass of the tube in the control volume and d_1 is the outer diameter of the tube. Therefore, the local wall heat flux is

$$q_w = -\frac{d_1^2 - d_2^2}{4 d_2} \rho_w C p_w \frac{\partial \bar{T}_w}{\partial t} \tag{6}$$

IV. Results and Discussion

A. Experimental Procedure and Test Case

Approximately 2 kg kerosene was prepared to a preset relatively low temperature in the first stage heater and at the same time the second stage heater was heated to a high temperature. The preheated kerosene was then driven by pressurized nitrogen at a given pressure and flowed through the test section. The total operation time was 13–15 s and it typically took 8 s for the kerosene flow reaching steady state. In the last 3 s of the operation, experimental data was used for the heat transfer analysis and the cracked products were collected for the composition analysis. Figure 4a demonstrates the time variation of the fuel pressure at the inlet and outlet of the second stage heater with the preset first- and second stage temperatures of 500 K and 915 K, respectively, and a mass flow rate of approximately 56 g/s.

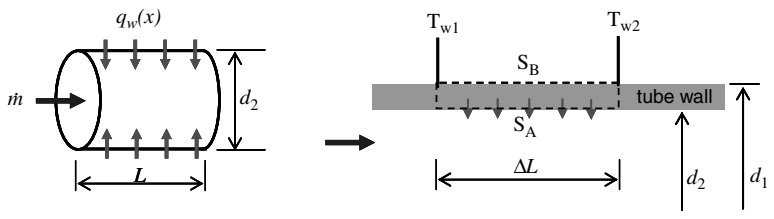

Fig. 3 Control volume analysis: a): a control volume for the fuel flow, and b) a control volume for the tube wall.

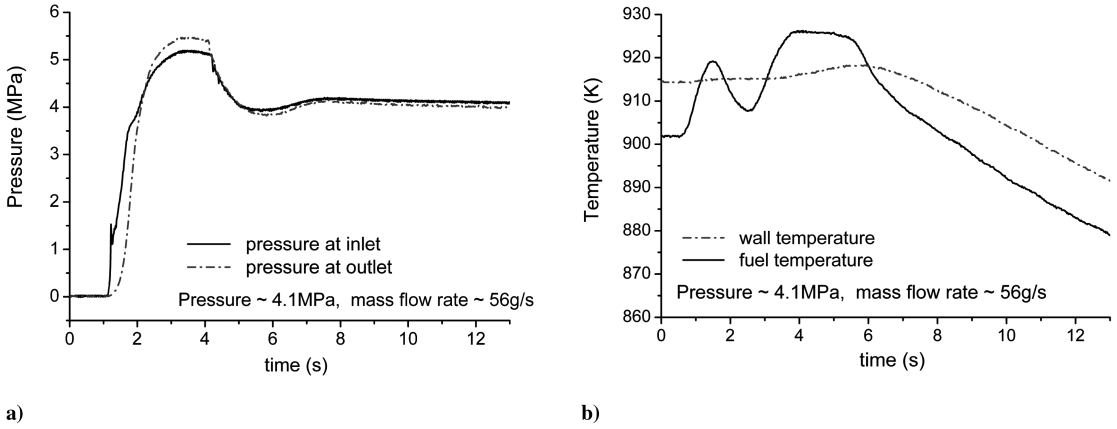

a) b)

Fig. 4 Time histories of inlet and outlet pressures and wall/fuel temperature of second stage heater: a) pressure, and b) temperature.

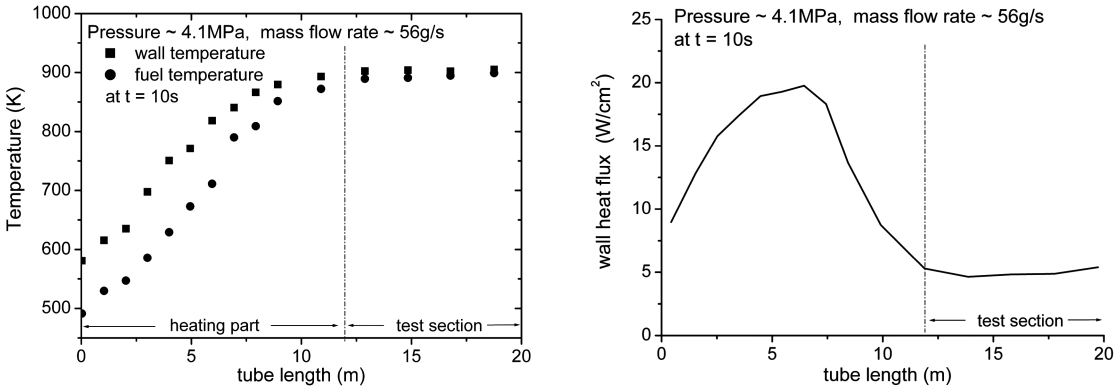

a) b)

Fig. 5 Graphs of a) axial distribution of the wall and fuel temperatures at $t = 10$ s, and b) axial distribution of the wall heat flux.

The kerosene was pressed into the second stage heater at a reference time $t = 1$ s by opening the pneumatic valve downstream of the first stage heater. From $t = 1$–4 s, the second pneumatic valve downstream of the second stage heater was closed to build up the pressure in the test section within a relatively short time. At $t = 4$ s, the second pneumatic valve was opened and kerosene started to flow through the test section.

As shown in Fig. 4a, the fuel pressure was stable after $t = 8$ s and the pressure drop through the tube of the second stage heater was quite small, approximately 80 KPa. Figure 4b presents the time history of the wall and fuel temperature at $x = 15$ m from the entrance of the second stage heater. It was found after $t = 8$ s, both the wall and fuel temperatures decrease linearly and at approximately the same rate. Note that the power of the second stage heater was shut off during the test time. The kerosene flow absorbs heat from the tube wall and causes the wall temperature drop. During the period of the products collection ($t = 10$–13 s), the fuel temperature was decreased by less than 12 K, leading to an average value of 887 K. The variation in the fuel temperature with time is quite small compared with the cracking temperature value.

Distributions of wall and fuel temperatures along the tube at $t = 10$ s are shown in Fig. 5a. As absorbing heat from the wall, the fuel temperature rises and approaches the wall temperature along the tube. After $x = 12$ m, the temperature difference between the fuel and the wall is very small and the convective heat transfer almost vanishes. In the region of $x = 12$–20 m, the increase in the fuel temperature along the tube is limited within 10 K, much smaller than the cracking temperature value. The downstream section of the tube serves as the test section where the fuel temperature is kept nearly constant and the convective heat transfer is negligible compared with the thermal cracking. Figure 5b plots the calculated wall heat flux distribution. In the upstream part of the tube, the main heat transfer is turbulent heat convection. In our previous work [9], it was found that the convective heat transfer of kerosene at supercritical pressures was affected strongly by its thermophysical properties and a heat transfer enhancement was observed as kerosene changed its state from compressed liquid to supercritical state. The details can be found in [9]. Compared with the upstream section of the tube, the heat transfer in the test section is dominated by endothermic cracking.

B. Fuel Conversion and Endothermicity

The fuel conversion is defined as the mass ratio of the gaseous products to the fuel feed $\eta = \frac{m_{\text{gas}}}{m_{k-\text{feed}}}$. Figure 6 shows the change of fuel conversion with fuel temperature at different residence times. As shown in Fig. 6, the cracking progresses as the temperature goes up.

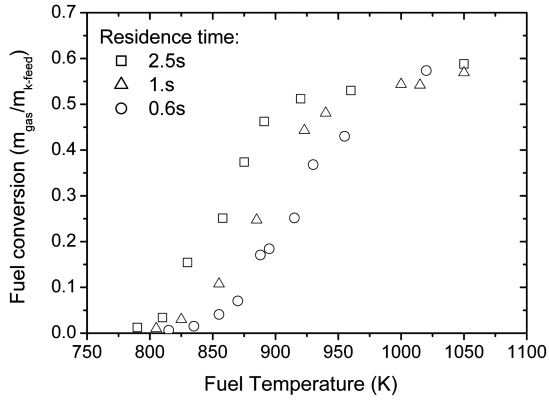

Fig. 6 Fuel conversion as functions of temperature and residence time.

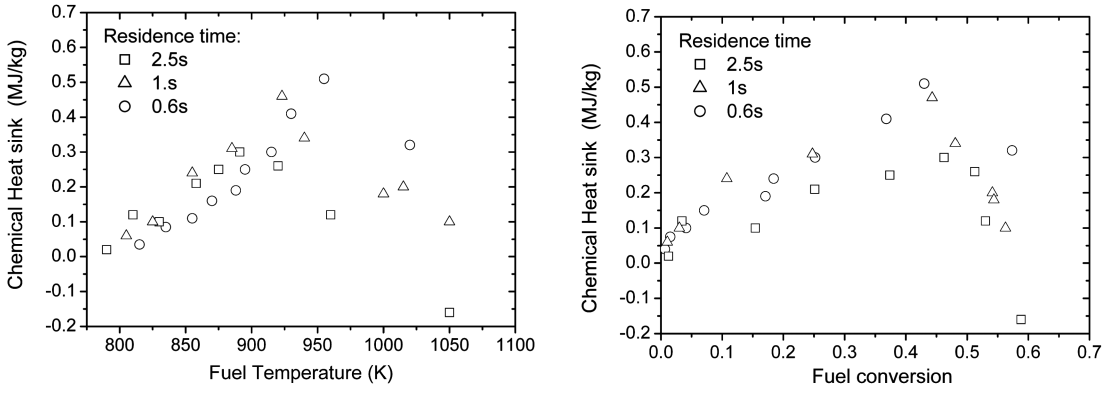

a) b)

Fig. 7 Chemical heat sink variation a) at varying temperatures and residence times, and b) at varying fuel conversion extents and residence times.

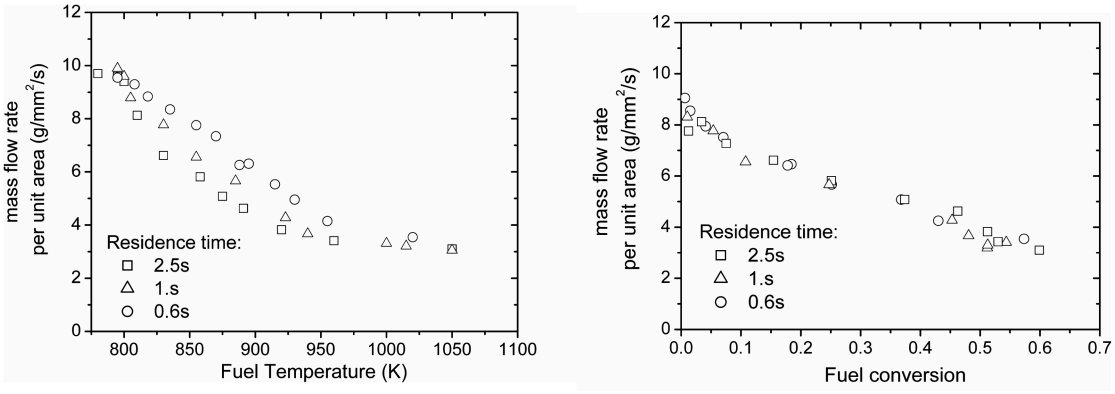

a) b)

Fig. 8 Normalized mass flow rate at varying residence times plotted as a function of a) fuel temperature and b) fuel conversion.

The active temperature range of the cracking was approximately from 800 to 1000 K and the fuel conversion was seen to level off beyond 1000 K. Figure 6 also indicates that thermal cracking at longer residence time begins at a relatively lower temperature, and at the same fuel temperature, it has a larger conversion than the cracking at shorter residence time. It was found that for the current pressure range of 3–4.5 MPa, the fuel conversion and other properties change slightly with pressure. Therefore, the following discussion will be focused on the effects of temperature and residence time.

Figure 7a illustrates the chemical heat sink obtained by Eq. (3) as functions of temperature and residence time. An important feature of Fig. 7a is that the chemical heat sink Δh_{endo} dose not increase monotonically with fuel temperature. A maximum heat sink exists at a fuel temperature of approximately 900–960 K and the fuel temperature corresponding to the maximum Δh_{endo} decreases with increasing residence time. For the long residence time of 2.5 s, at a high temperature of 1050 K the chemical heat sink even becomes negative, indicating exothermicity of the resulting reactions. The decrease in the chemical heat sink at relatively high temperatures can be explained by the change in the cracking products with temperature. The results of gas chromatography discussed in Sec. IV.D will show that more saturated hydrocarbons such as methane are produced as the fuel temperature increases further. It is known that formation of saturated hydrocarbons is generally exothermic in nature. Therefore, at increasingly high fuel temperatures the cracking tends to be exothermic and the chemical heat sink decreases.

Figure 7b shows the same results plotted via the extent of fuel conversion. At the same conversion, the shorter residence time case leads to a larger chemical heat sink, and for the current test conditions, the maximum value of Δh_{endo} was found to be approximately 0.5 MJ/kg at a fuel conversion of 0.45 and at a residence time of approximately 0.6 s. This maximum value is smaller than the value for JP-7 reported in [1,4], which can be attributed to the differences in the fuel composition and the residence time. Because the total sensible heat capacity of China No. 3 kerosene at a temperature range of 300–800 K is approximately 1.4 MJ/kg, the heat sink of 0.5 MJ/kg due to endothermic cracking is therefore considerably important.

C. Fuel Mass Flow Rate

The measured mass flow rate divided by the cross area of the sonic nozzle throat ($\frac{\dot{m}}{A^*}$) are shown in Figs. 8a and 8b as a function of fuel temperature and fuel conversion, respectively. In Fig. 8, all the data at

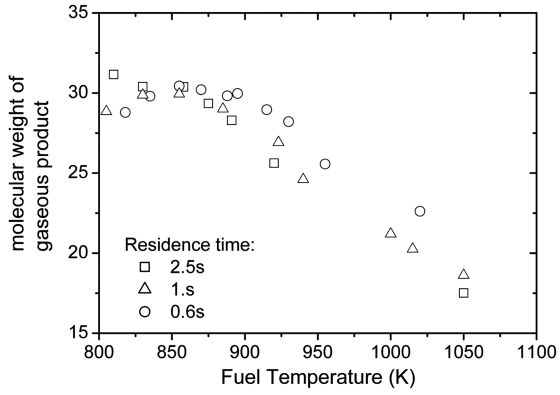

Fig. 9 Molecular weight of the gaseous product as functions of temperature and residence time.

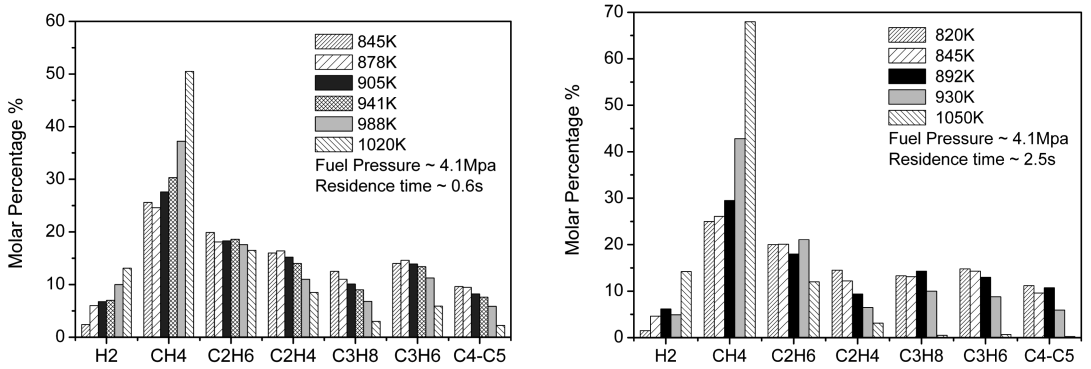

a) b)

Fig. 10 Compositions of the gaseous products at varying temperatures: a) residence time is 0.6 s, and b) residence time is 2.5 s.

varying pressures were normalized with a reference pressure of 3.5 MPa. It was found that the mass flow rate decreased with increasing fuel temperature because of the reduction in the average molecular weight of the cracked mixture $\bar{\mu}$, as indicated in Eq. (7):

$$\frac{\dot{m}}{A^*} = \frac{p}{\sqrt{\hat{R}T/\bar{\mu}}} cf(\gamma) \tag{7}$$

where $f(\gamma) = \sqrt{\gamma(\frac{2}{1+\gamma})^{\frac{(\gamma+1)}{(\gamma-1)}}}$, $\hat{R}$ is the universal gas constant, γ is 1.2, and c is a discharge coefficient. The value of c is taken as 0.91, accounting for the pressure loss through the sonic nozzle.

Dependency of $\frac{\dot{m}}{A^*}$ on residence time is shown in Fig. 8a. Scattering of the data with varying residence time is observed in the figure. Shorter residence time corresponds to relatively larger mass flow rate, but this dependency diminishes as fuel temperature exceeds 1000 K. Such a trend can be explained by the changes in fuel conversion and average molecular weight of the cracking mixture with increasing temperature for varying residence times. When plotting the same mass flow rate data against the fuel conversion η, it is seen from Fig. 8b that all data collapse into a single curve, thereby indicating that η is a better correlation parameter than the fuel temperature.

D. Results of Gas Chromatography

The average molecular weight of the gaseous products $\bar{\mu}_g$ is plotted in Fig. 9 at varying fuel temperatures and residence times, and $\bar{\mu}_g$ was found to decrease as fuel temperature is increased. At the highest test temperature of approximately 1050 K, $\bar{\mu}_g$ is only 17, indicating large percentage of small molecules in the product such as methane. $\bar{\mu}_g$ was also seen to be dependent slightly on the residence time, and larger residence time leads to smaller value of $\bar{\mu}_g$.

The major gaseous products due to thermal cracking were hydrogen, methane, ethane, propane, ethylene, and propylene. Figure 10 compares the compositions (in molar percentage) of the gaseous products at varying fuel temperatures, and at two residence times of 0.6 and 2.5 s. It is seen from Fig. 10 that increasing fuel temperature generally increases the percentage of paraffin hydrocarbons. The molar percentage of methane was 50% at 1020 K for the residence time of 0.6 s and it was as high as 70% at 1050 K for the residence time of 2.5 s. The large percentage of methane in the gaseous product

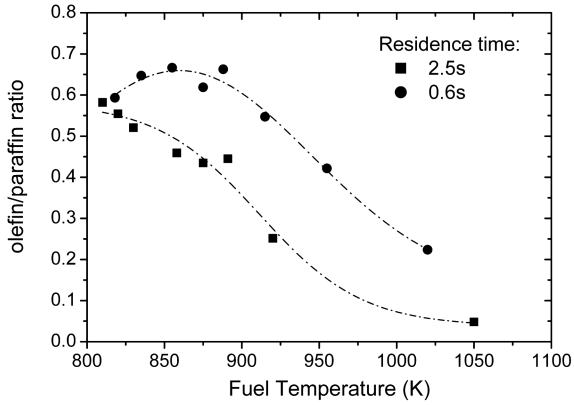

Fig. 11 Olefin/paraffin ratio variations at varying fuel temperatures and residence times.

indicates significant reduction in the endothermicity of cracking and it is consistent with the change of chemical heat sink as shown in Fig. 7. The "olefin/paraffin" ratio has been used to represent endothermicity by many studies [5,14]. A larger olefin/paraffin ratio indicates a better endothermicity. Using the data of Fig. 10, the olefin/paraffin ratio λ defined by [(ethylene + propylene)/(methane+ ethane + propane)] is given in Fig. 11 as a function of fuel temperature for two different residence times. It is seen that the variation of the olefin/paraffin ratio at the two residence times gives different trends; λ at residence time of 0.6 s yields a peak value at a fuel temperature of approximately 880 K, while for the long residence time of 2.5 s, it simply decreases with increasing fuel temperature. Figure 11 also shows that at the same fuel temperature, the shorter residence time leads to significantly larger olefin/paraffin ratio, indicating that the cracking process is more endothermic at shorter residence time. For the two residence times investigated, the overall decrease in the olefin/paraffin ratio with fuel temperature can explain the phenomena observed in Fig. 7.

Compositions of the liquid product were also analyzed with gas chromatography and the results are listed in Tables 1 and 2. Table 1 gives the main compositions (in molar percentage) of the liquid product at a fuel temperature of $T_f = 950$ K, a fuel pressure of $P_f = 4.1$ MPa, and with a residence time of 0.6 s. The species com-

Table 1 Compositions of the liquid product at $T_f = 950$ K, $P_f = 4.1$ MPa, and residence time =0.6 s

Toluene	Benzene	Naphthalene	O-xylene	1-Methyl-Naphthalene
(C_7H_8)	(C_6H_6)	($C_{10}H_8$)	(C_8H_{10})	($C_{11}H_{10}$)
22.5%	14.9%	12.5%	8.5%	7.8%
2-Methyl-Naphthalene	Styrene	1,2,3-Trimethyl-Benzene	Ethylbenzene	Indene
($C_{11}H_{10}$)	(C_8H_8)	(C_9H_{12})	(C_8H_{10})	(C_9H_8)
5.3%	5.96%	2.72	2.2%	2.1%

Table 2 Compositions of the liquid product at $T_f = 1050$ K, $P_f = 4.1$ MPa, and Residence Time = 1 s

Benzene (C_6H_6)	Toluene (C_7H_8)	Naphthalene ($C_{10}H_8$)	1-methyl-Naphthalene ($C_{11}H_{10}$)	2-methyl-Naphthalene ($C_{11}H_{10}$)
15.15%	18.3%	40.94%	16.36%	9.24%

ponents are mainly benzene-based and naphthalene-based aromatic hydrocarbons. It can be explained partly by the ring-contraction products at high (supercritical) pressures (so-called *cage effect* [7,15]). Table 2 shows the liquid compositions at a fuel temperature of $T_f = 1050$ K, a fuel pressure of $P_f = 4.1$ MPa, and with a residence time of 1 s. A large percentage of naphthalene was noted, which could be associated with significantly increase in carbon formation at high temperatures.

V. Conclusions

In this study, thermal cracking of China No. 3 aviation kerosene in a heated tube was investigated at a temperature range of 780–1050 K, a pressure range of 3–4.5 MPa, and a residence time range of 0.6–3 s. Heat transfer analysis based on the energy balance for control volumes of the kerosene flow and the tube wall was used to determine the chemical heat sink (endothermicity). With the composition results obtained using gas chromatography, the cracking and endothermicity properties were discussed. Listed below are several conclusions drawn from this work.

1) Thermal cracking of China No. 3 kerosene started at a temperature of approximately 800 K. This critical temperature was noted to increase as residence time was decreased. For the conditions studied, the active cracking temperature was found to be in the range of 800–1000 K.

2) The chemical heat sink does not always increase with fuel temperature; a maximum endothermicity was found to occur at a fuel temperature of approximately 900–960 K, which varied with different residence times. For the current operation condition, the maximum heat sink was found to be approximately 0.5 MJ/kg with a 45% fuel conversion.

3) The mass flow rate of the thermally cracked kerosene decreased with increasing fuel temperature and residence time. Fuel conversion was found to be a better parameter than fuel temperature for the mass flow rate correlation.

4) Speciation results demonstrated that the main gaseous products were methane, hydrogen, ethane, and ethylene. As temperature and residence time were increased, the methane percentage rose to more than 50% and the increased percentage of saturated hydrocarbons from cracking led to significant reduction in endothermicity.

5) The major compositions of the liquid products were found to be benzene-based and naphthalene-based aromatic hydrocarbons, and a considerably large percentage of naphthalene was observed at a temperature of 1050 K.

Acknowledgments

This work was funded by the Natural Science Foundation of China under Contract No. 10902115. The authors would like to thank Xiangwen Zhang of Tianjin University for his experimental efforts in gas chromatography. The authors also thank Chenxi Jiang, Ying Li, and Xuesong Wei for their technical support.

References

[1] Lander, H., and Nixon, A. C., "Endothermic Fuels for Hypersonic Vehicles," *Journal of Aircraft*, Vol. 8, No. 4, 1971, pp. 200–207. doi:10.2514/3.44255

[2] Huang, H., Spadaccini, L. J., and Sobel, D. R., "Fuel-Cooled Thermal Management for Advanced Aero-Engines," *Journal of Engineering for Gas Turbines and Power*, Vol. 126, No. 2, 2004, pp. 284–293. doi:10.1115/1.1689361

[3] Crynes, B. L., and Albright, L. F., "Thermal Cracking," *Encyclopedia of Physical Science and Technology*, Vol. 3, Academic Press, New York, pp. 768–785.

[4] Edwards, T., and Anderson, S., "Results of High Temperature JP-7 Cracking Assessment," AIAA Paper 1993-0806, 1993.

[5] Edwards, T., "Recent Research Results in Advanced Fuels," *Preprints: American Chemical Society, Division of Petroleum Chemistry*, Vol. 41, No. 2, 1996, pp. 481–487.

[6] Edwards, T., "Cracking and Deposition Behavior of Supercritical Hydrocarbon Aviation Fuels," *Combustion Science and Technology*, Vol. 178, Nos. 1-3, 2006, pp. 307–334. doi:10.1080/00102200500294346

[7] Stewart, J., Brezinsky, K., and Glassman, I., "Supercritical Pyrolysis of Decalin, Tetralin and *n*-decane at 700–800 K Product Distribution and Reaction Mechanism," *Combustion Science and Technology*, Vol. 136, No. 1, April, 1998, pp. 373–390. doi:10.1080/00102209808924178

[8] Fan, X-J., Yu, G., Li, J-G., Lu, X-N., Zhang, X-Y., and Sung, C. J., "Combustion and Ignition of Thermal Cracked Kerosene in Supersonic Model Combustors," *Journal of Propulsion and Power*, Vol. 23, No. 2, 2007, pp. 317–324. doi:10.2514/1.26402

[9] Zhong, F-Q., Fan, X-J., Yu, G., Li, J-G., and Sung, C. J., "Heat Transfer of Aviation Kerosene at Supercritical Conditions," *Journal of Thermophysics and Heat Transfer*, Vol. 23, No. 3, 2009, pp. 543–550.

[10] Fan, X., Yu, G., Li, J. G., and Sung, C. J., "Flow Rate Analyses and Calibrations of Kerosene Cracking for Supersonic Combustion," AIAA Paper 2005-3555, 2005.

[11] Zhong, F-Q., Fan, X-J., Yu, G., and Li, J-G., "Thermal Cracking of Aviation Kerosene for Scramjet Applications," *Science in China Series E, Technological Sciences*, Vol. 52, No. 9, 2009, pp. 2644–2652. doi:10.1007/s11431-009-0090-8

[12] Fan, X-J., Yu, G., Li, J-G., Zhang, X-Y., Yue, L.-J., and Sung, C. J., "Effects of Entry Conditions on Cracked Kerosene-Fueled Supersonic Combustor Performance," *Combustion Science and Technology*, Vol. 179, No. 10, 2007, pp. 2199–2217. doi:10.1080/00102200701386198

[13] Ely, J. F., and Huber, M. L., "NIST Standard Reference Database 4-NIST Thermophysical Properties of Hydrocarbon Mixtures," National Inst. of Standards, Gaithersburg, MD, Feb., 1990.

[14] Dardas, Z., Suer, M. G., Ma, Y. H., and Moser, W. R., "A Kinetic Study of *n*-Heptane Catalytic Cracking over a Commercial Y-Type Zeolite under Supercritical and Subcritical Conditions," *Journal of Catalysis*, Vol. 162, No. 2, 1996, pp. 327–338. doi:10.1006/jcat.1996.0290

[15] Yu., J., and Eser, S., "Thermal Decomposition of Jet Fuel Model Compounds Under Near-Critical and Supercritical Conditions 2. Decalin and Tetralin," *Industrial and Engineering Chemistry Research*, Vol. 37, No. 12, 1998, pp. 4601–4608. doi:10.1021/ie980302y